Supplementary Material (ESI) for Chemical Communications

Supporting Information

New Trimeric Polyoxotungstate Aggregates Based on $[P_2W_{12}O_{48}]^{14-}$ Building Blocks

Zhi-Ming Zhang,[a] Shuang Yao,[a] Yang-Guang Li,[a,*] Yong-Hui Wang,[a] Yan-Fei Qi,[a] and En-Bo Wang [a,*]

CONTENTS

1. Supplementary Structural Figures of Compounds 1-3

2. Experimental Section

3. Synthetic Discussion

4. Aqueous Solution stability of Polyoxoanions 1a-3a

5. Electrochemistry and Electrocatalysis of 1-3

6. Magnetic Properties of Compounds 1-3

7. Other Characterizations of Compounds 1-3

1. Supplementary Structural Figures of Compounds 1-3

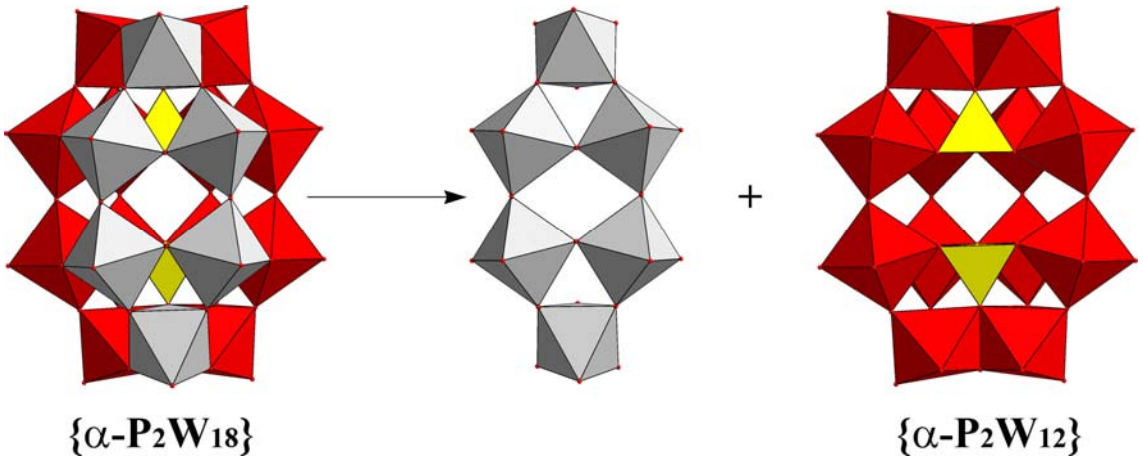

Scheme S1. Schematic presentation of $\{P_2W_{12}\}$ derived from the Dawson-type $[P_2W_{18}O_{62}]^{6-}$.

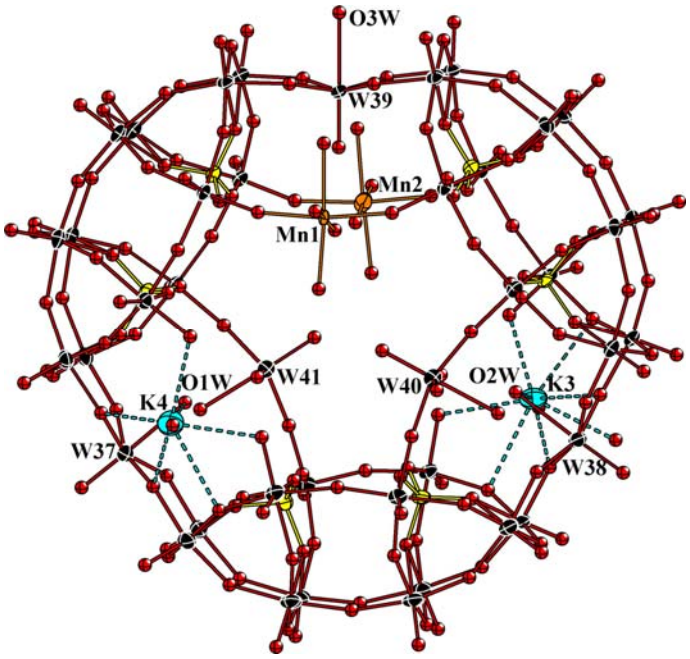

Fig. S1. ORTEP drawing of **1a** with thermal ellipsoids at 50% probability. The inner K^+ ions and water molecules are omitted for clarity.

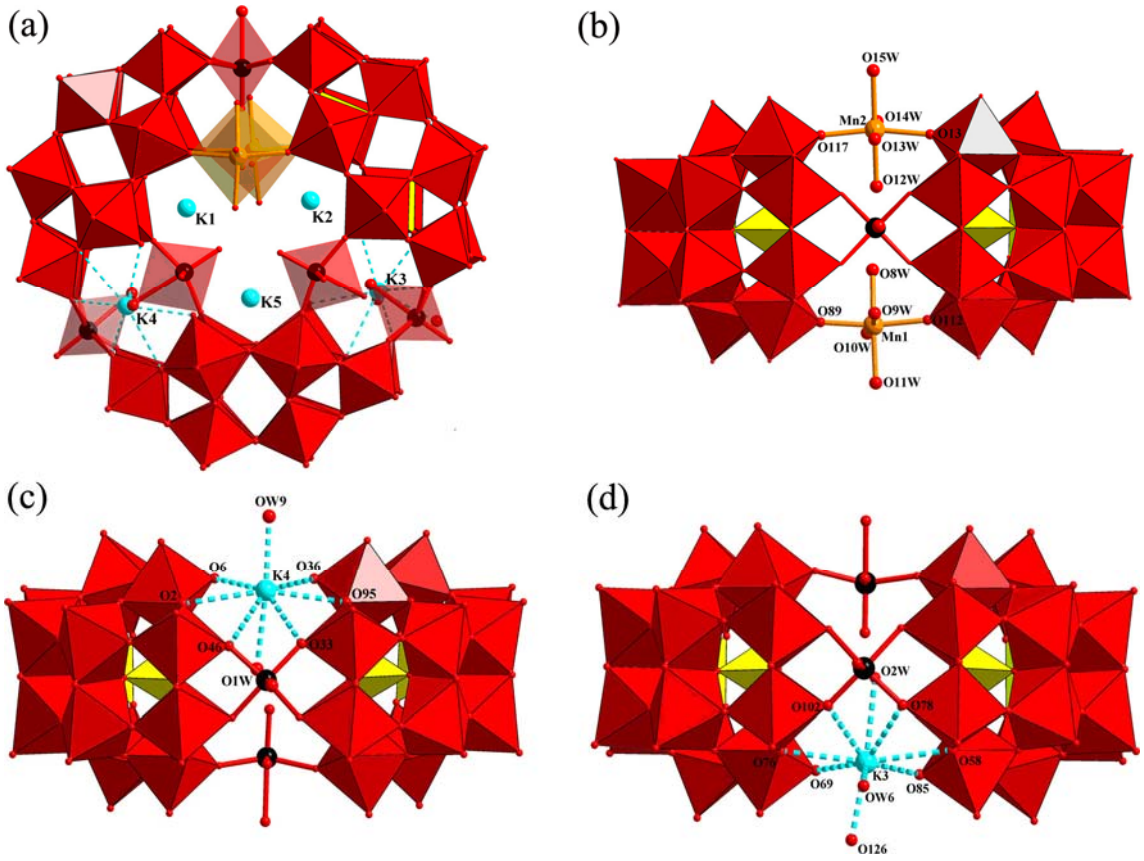

Fig. S2. Polyhedral and ball-and-stick representation of polyoxoanion **1a** and the connection modes in the three linking sites of **1a**.

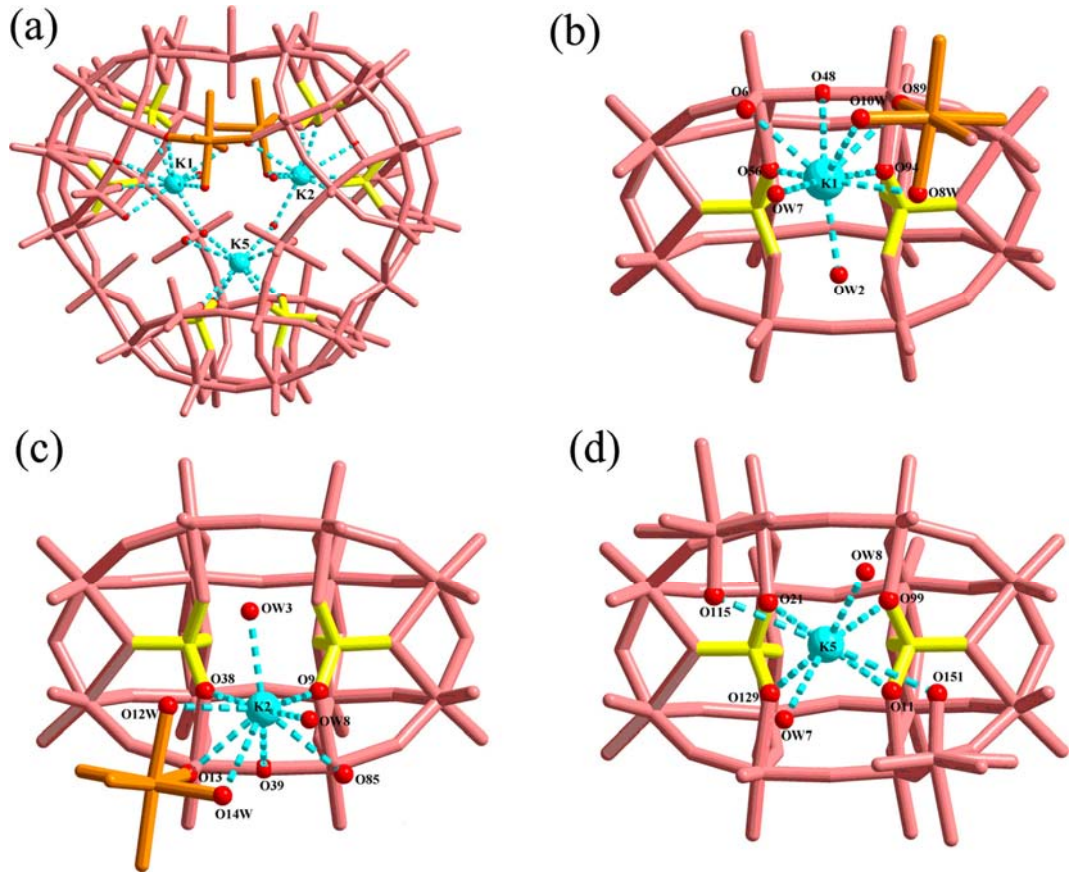

Fig. S3. Ball-and-stick representation of the coordination modes of three K^+ cations sealed in polyoxoanion **1a**.

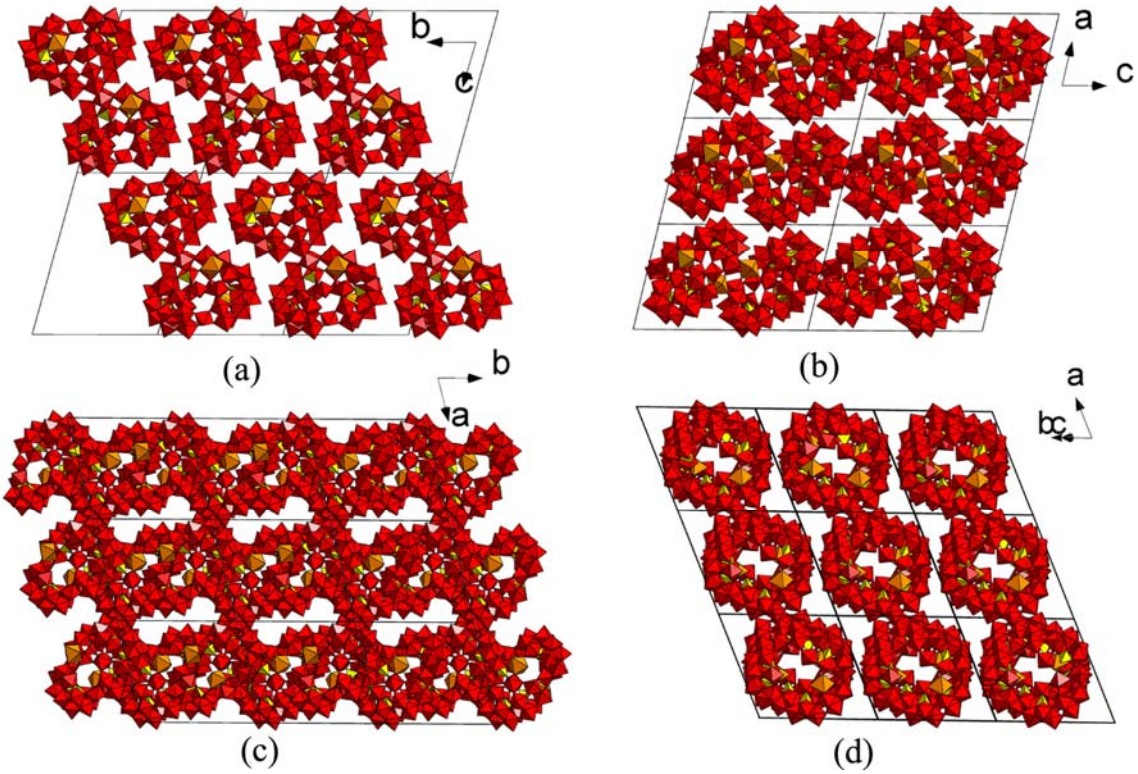

Fig. S4. Polyhedral representation of the packing arrangements of **1** viewed along different directions. K^+, Na^+ and the lattice H_2O molecules are omitted for clarity.

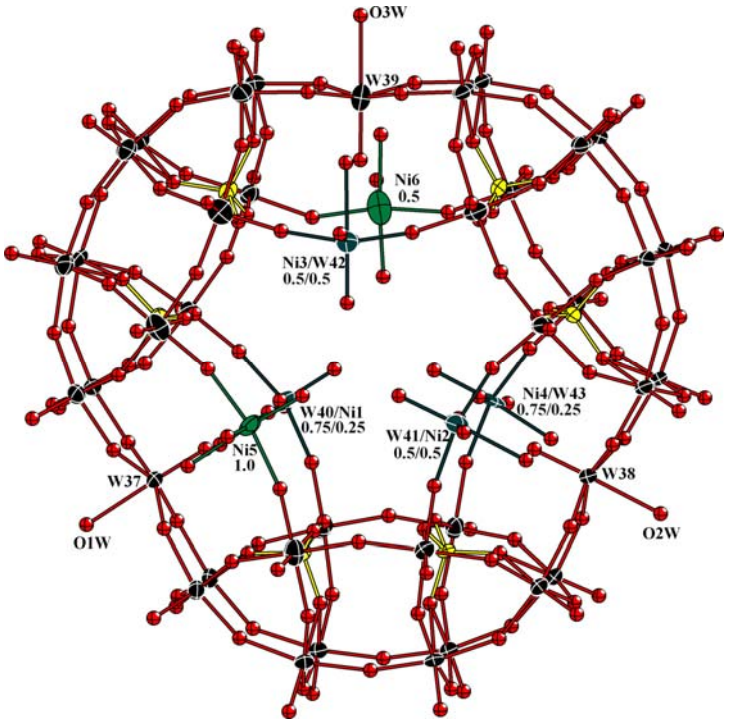

Fig. S5. ORTEP drawing of **2a** with thermal ellipsoids at 50 % probability. The inner Na^+ ions and water molecules are omitted for clarity.

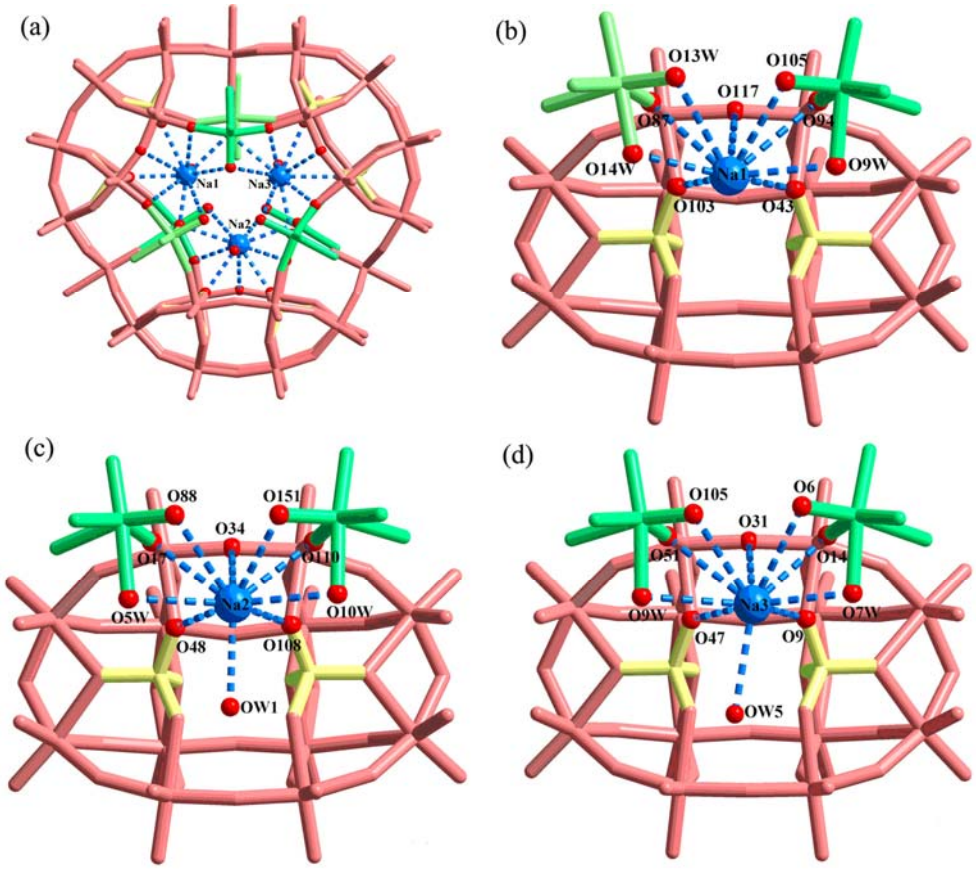

Fig. S6. Ball-and-stick representation of the coordination modes of three sodium cations encapsulated in **2a**.

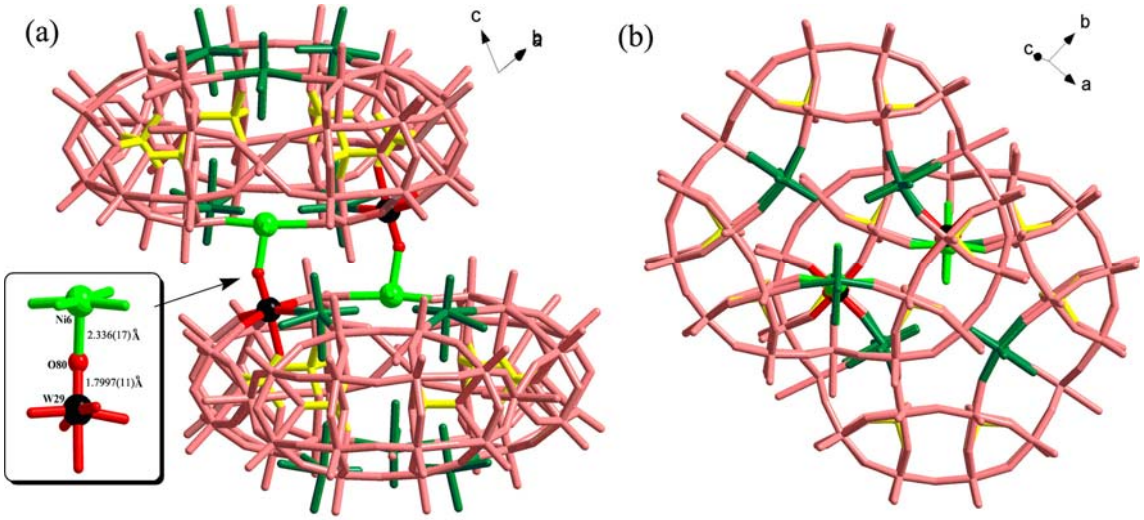

Fig. S7. Ball-and-stick representation of dimeric **2a** via two W-O-Ni bonds.

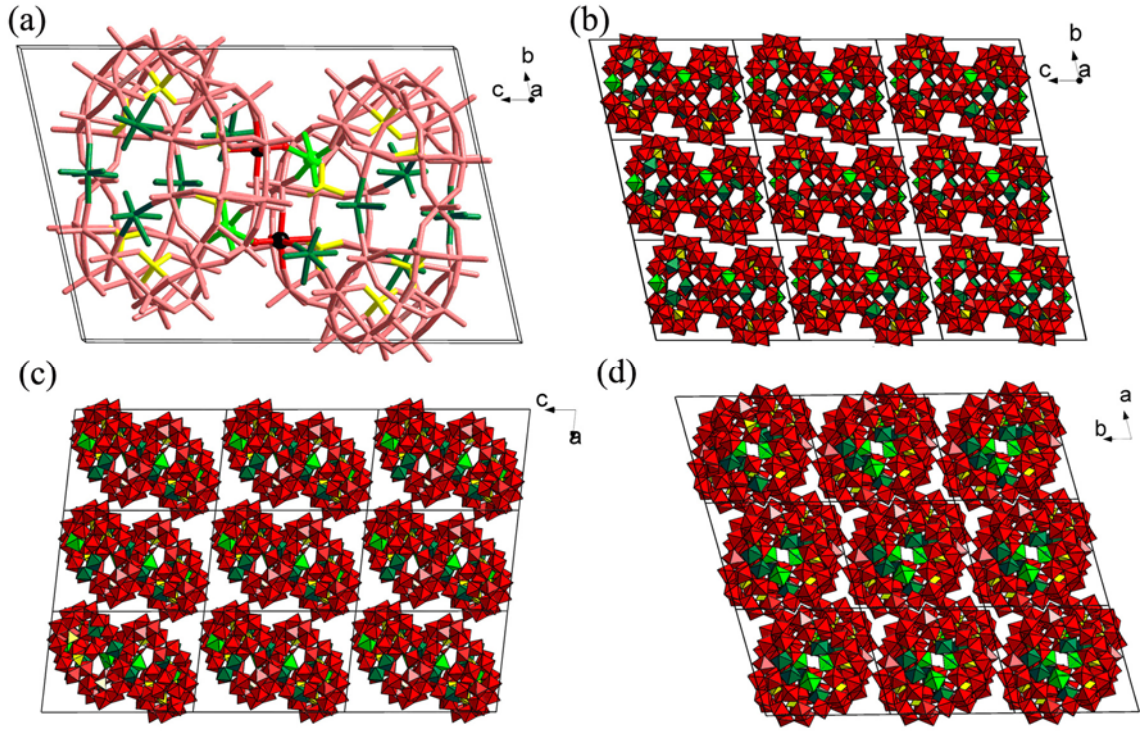

Fig. S8. (a) Ball-and-stick view of the dimeric **2a** in one unit cell; (b) (c) (d) packing arrangements of **2** viewed along different directions. K^+, Na^+ and the lattice H_2O molecules are omitted for clarity.

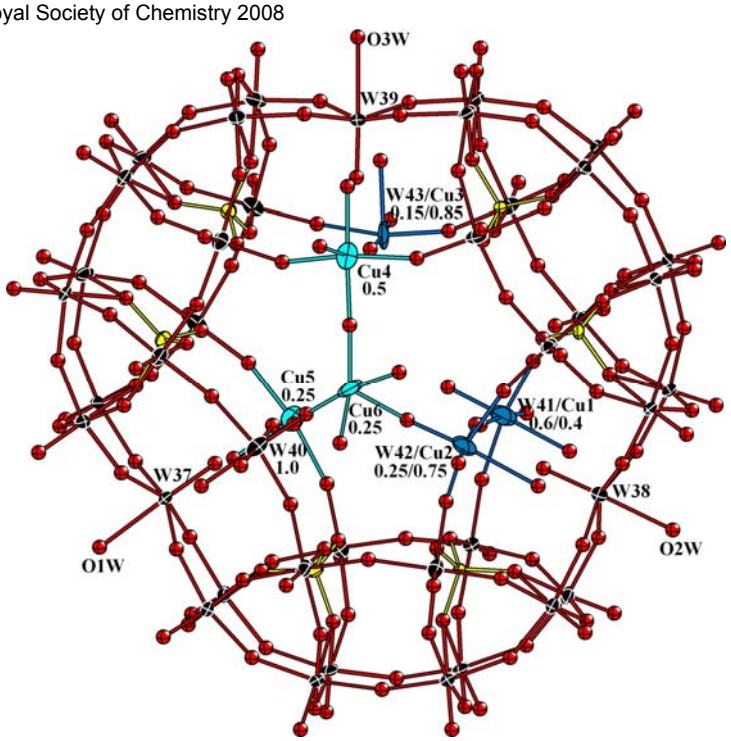

Fig. S9. ORTEP drawing of **3a** with thermal ellipsoids at 50% probability. The inner Na^+ ions and water molecules are omitted for clarity.

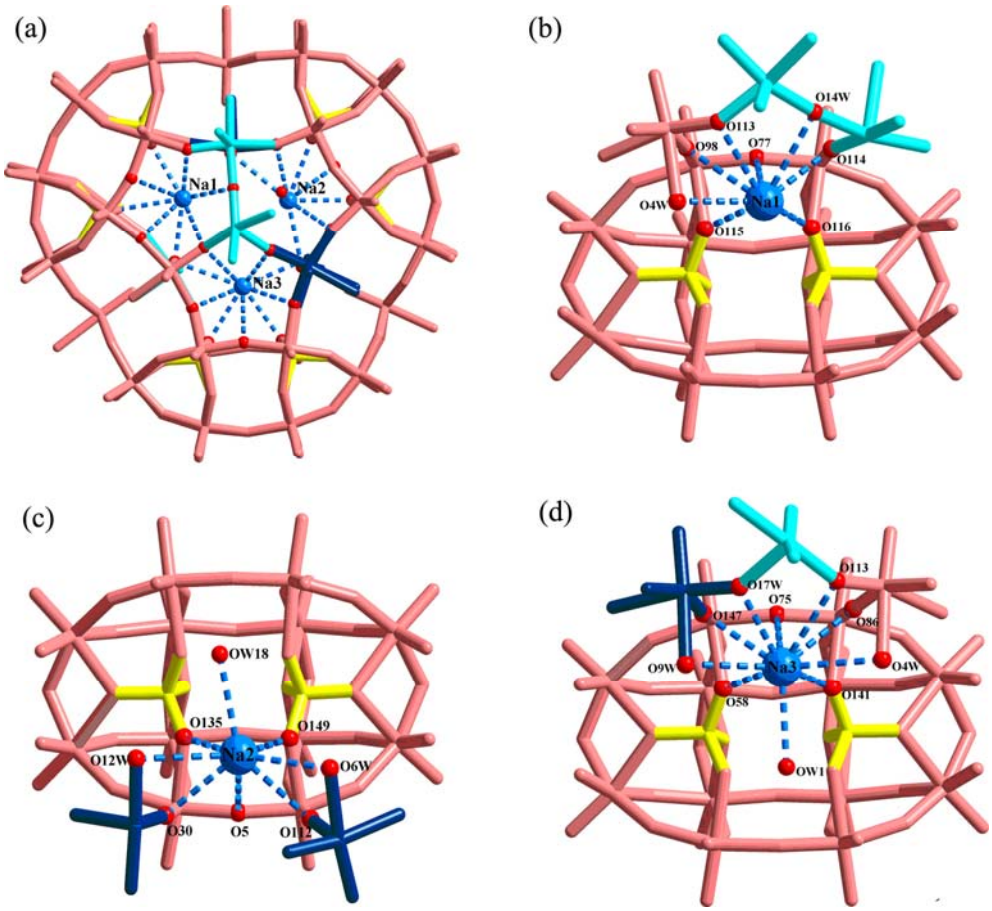

Fig. S10. View of the coordination modes of three Na^+ cations sealed in polyoxoanion **3a**.

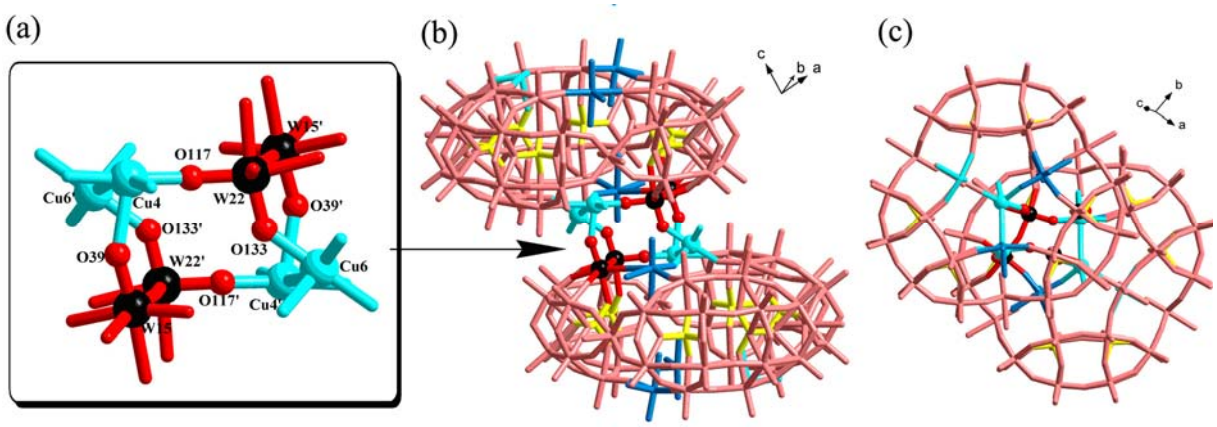

Fig. S11 Ball-and-stick representation of dimeric **2a**.

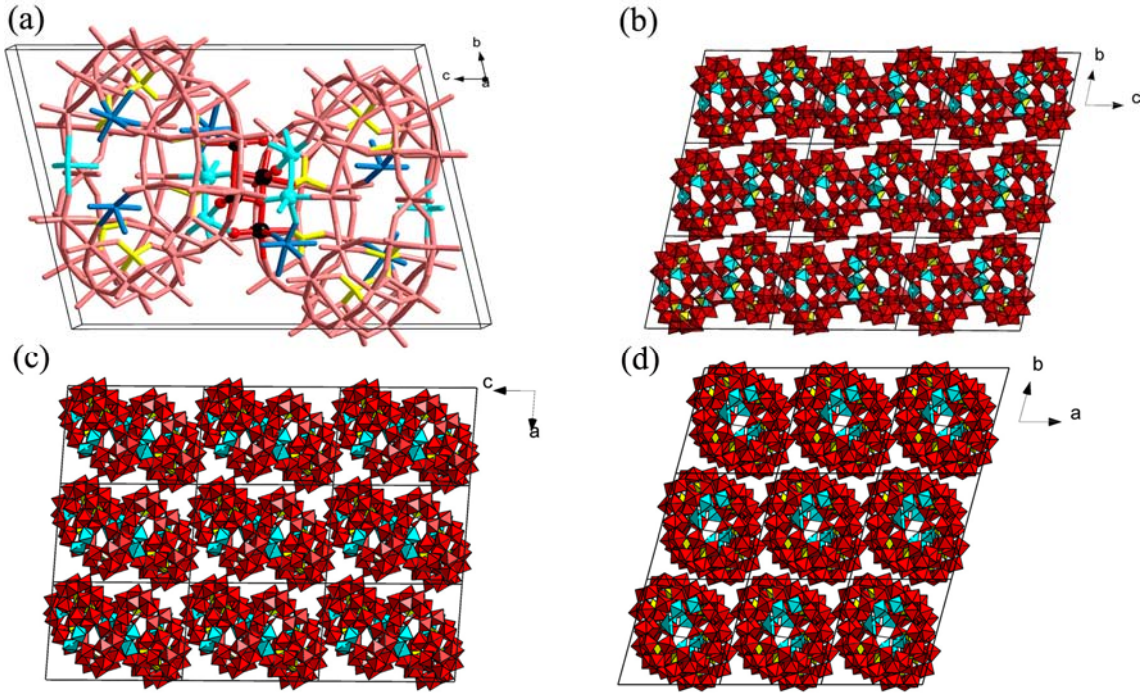

Fig. S12. (a) Ball-and-stick view of a dimeric **3a** in one unit cell; (b) (c) (d) Packing arrangement of **3** viewed along different directions. K^+, Na^+ and the lattice H_2O molecules are omitted for clarity.

2. Experimental Section

2.1. Materials and Methods: All chemicals were commercially purchased and used without further purification. $K_{12}[H_2P_2W_{12}O_{48}]\bullet 24H_2O$ was synthesized according to the literature method.[1] Elemental analyses of K, Na, Li, P, W, Mn, Ni and Cu were performed by a Leaman inductively coupled plasma (ICP) spectrometer. Water contents were determined by TG analyses on a Perkin–Elmer TGA7 instrument in flowing N_2 with a heating rate of 10 $°C\cdot min^{-1}$. IR spectra were recorded in the range of 400–4000 cm^{-1} on an Alpha Centaurt FT/IR Spectrophotometer with pressed KBr pellets. UV-Vis absorption spectra were obtained using a 752 PC UV-Vis spectrophotometer. Magnetic susceptibility measurements were obtained on finely grounded polycrystalline samples (grease restricted) with the use of a Quantum Design SQUID magnetometer MPMS-XL. Experimental data were corrected for the sample holder and for the diamagnetic contribution calculated from Pascal constants.[2]

2.2. Crystallography: Data collection was performed at 150(2) K on a Rigaku R-axis Rapid IP diffractometer with graphite-monochromated $Mo_{K\alpha}$ radiation (λ = 0.71073 Å) and IP technique. Suitable crystals were affixed to the end of a glass fiber using silicone grease and transferred to the goniostat. Multi-scan absorption correction was applied. The structures of **1**–**3** were solved by the direct method and refined by the full-matrix least-squares method on F^2 using the SHELXTL-97 crystallographic software package.[3] During the refinement of **1**–**3**, there were a number of short connections between OW(water)...O(POM) in the range of 2.60~2.90 Å, suggesting the extensive H-bonding interactions between lattice water molecules and the POMs. However, the H atoms between them could not be determined from the difference Fourier maps due to the limited quality of the data. All H atoms on water molecules were directly included in the molecular formula. All structures possess apparent disorders in the range of counter-cations and lattice water molecules, preventing a more precise structural analysis. However, none of these deficiencies affects the structural details and reliability of the polyoxoanion structures. In **1**–**3**, only partial lattice water molecules can be accurately assigned from the residual electron peaks, while the rest were directly included in the molecular formula based on the elemental analyses and TG analyses.

2.3. General Electrochemical Materials and Methods. Thrice-distilled water was used throughout the experiments. A 0.4 M CH_3COONa+CH_3COOH solution (pH 4) for **1** and a 1M LiCl + 0.5M H_2SO_4 (pH 2.5) solution for **2** and **3** were used during the experiments. Solutions were deaerated by pure argon bubbling prior to the experiments and the electrochemical cell was kept under an argon atmosphere throughout the experiment.

A CHI 660 electrochemical workstation connected to a Pentium-Ⅳ personal computer was used for control of the electrochemical measurements and for data collection. A conventional three-electrode system was used. The working electrode was a glassy carbon (GC), the reference electrode was the Ag/AgCl electrode, and platinum wire was used as a counter electrode. All potentials were measured and reported versus the Ag/AgCl. The solution

concentrations of **1-3** were all 10^{-3} M. A pHS-25B type pH meter was used for pH measurement. All the experiments were carried out at room temperature (25–30 °C).

References

1 R. Contant, *Inorg. Synth.,* 1990, **27**, 104.

2 E.A. Boudreaux, L. N. Mulay, *Theory and Applications of Molecular Paramagnetism, Eds. John Wiley & Sons,* New-York, **1976**.

3 G. M. Sheldrick, *SHELXL97, Program for Crystal Structure Refinement*, University of Göttingen: Göttingen, Germany, **1997**; G. M. Sheldrick, *SHELXS97, Program for Crystal Structure Solution*, University of Göttingen: Göttingen, Germany, **1997**.

3. Synthetic Discussion

The hexavacant Dawson-type polyoxoanion $[P_2W_{12}O_{48}]^{14-}$ (abbreviated by $\{P_2W_{12}\}$) possesses relatively high capability of combining metal ions and represents one of the excellent building blocks for the assembly of new nanoscale crown-type aggregates. During the preparation, it was found that $\{P_2W_{12}\}$ units are inclined to condense into the tetrameric $\{P_8W_{48}\}$.[1] Thus, the synthesis of new $\{P_2W_{12}\}$-based crown-type aggregates must firstly avoid the formation of this tetramer. In our experiments, extra $Na_2WO_4{\cdot}2H_2O$ was introduced into the reaction system containing $[P_2W_{12}O_{48}]^{14-}$ and various transition metal salts, which successfully prevented the tetrameric polymerization. Hence three new trimeric crown-type compounds **1-3** were isolated**.** In such a reaction system, there are four key synthetic conditions that affect the experimental results: pH value, ionic concentration, reaction temperature and the evaporation rate of the solvent. Firstly, compound **1** was isolated from the pH 4 acetate buffer solution, while compounds **2-3** could be synthesized from the pH 1.5 ~ 2.5 reaction system. Out of this pH conditions, no compounds **1-3** can be obtained. Secondly, the transition metal ions were superfluously used in all three reaction system, otherwise only Dawson-type $[P_2W_{18}O_{62}]^{6-}$ were isolated. Thirdly, the reaction temperature should keep lower than 50 °C, otherwise $[P_2W_{18}O_{62}]^{6-}$ will be obtained from this reaction system. Finally, slow evaporation must be kept for the filtrate and the crystals of **1-3** are usually isolated after two weeks. Too quick crystallization will lead to a large amount of light-yellow byproducts of $[P_2W_{18}O_{62}]^{6-}$ and obviously reduce the yields of compounds **1-3**.

1 (a) R. Contant, A. Tézé, *Inorg. Chem.,* **1985**, *24*, 4610; (b) R. Contant, *Inorg. Synth.,* **1990**, *27*, 104.

4. Aqueous Solution stability of Polyoxoanions 1a-3a

4.1. Gel Filtration Chromatography. Gel filtration chromatography analysis was performed on the three title compounds by the use the 0.4 M CH_3COONa+CH_3COOH (pH 4) elution buffer for **1** and 1 M LiCl + 0.5 M H_2SO_4 (pH 2.5) elution buffer for **2** and **3** in a 40 cm × 1 cm^2 Sephadex G-50 (fine) column, which allows the separation of species with molecular masses in the range 500 to 10000 g mol^{-1}.[1] The analytical results revealed that compound **1** was eluted far earlier than $[P_2W_{15}Mo_2VO_{62}]^{8-}$ (ionic mass = 4055) and no other species were detected after $[P_2W_{15}Mo_2VO_{62}]^{8-}$ was eluted. This experimental result suggests that the ionic mass of **1a** (ionic mass = 10521) is larger than that of $[P_2W_{15}Mo_2VO_{62}]^{8-}$, and no decomposition of trimeric **1a** into dimer or monomer happens in the aqueous solution. Further, compounds **2** and **3** were also eluted far earlier than $[P_2W_{15}Mo_2VO_{62}]^{8-}$, indicating that their molecular masses are larger than this reference polyoxoanion and even larger than the upper separation limit of Sephadex G-50 (10 000 $gmol^{-1}$). These experiments confirm that polyoxoanions **2a-3a** still keep the trimeric crown-type structures in aqueous solutions.

1 (a) B. S. Bassil, U. Kortz, A. S. Tigan, J. M. Clemente-Juan, B. Keita, P. de Oliveira, L. Nadjo, *Inorg. Chem.,* **2005**, *44*, 9360; (b) B. Keita, P. Oliveira, L. Nadjo, U. Kortz, *Chem. Eur. J.,* **2007**, *13*, 5480.

4.2. Cyclic Voltammetric (CV) and UV-vis spectrum. The aqueous solution stabilities of polyoxoanion **1a-3a** have also been investigated by the CV and UV-vis spectra. Polyoxoanion **1a** was dissolved in the pH 4 (0.4 M CH_3COONa+CH_3COOH) buffer solution and **2a-3a** were dissolved in the pH 2.5 (1 M LiCl + 0.5 M H_2SO_4) solution, respectively. All above solutions were kept at room temperature. The cyclic voltammetric behaviors of these solutions were detected per 24 h. After a 5-day's checking, these solutions can be well stored and no voltammetric characteristics have ever changed (see Fig. S13a, S14a and S15a). Further, the UV-vis spectra of the above solutions were checked simultaneously and no changes were observed during five days (see Fig. S13b, S14b and S15b). These characterizations further confirm that polyoxoanions **1a-3a** are structurally stable in the aqueous solution.

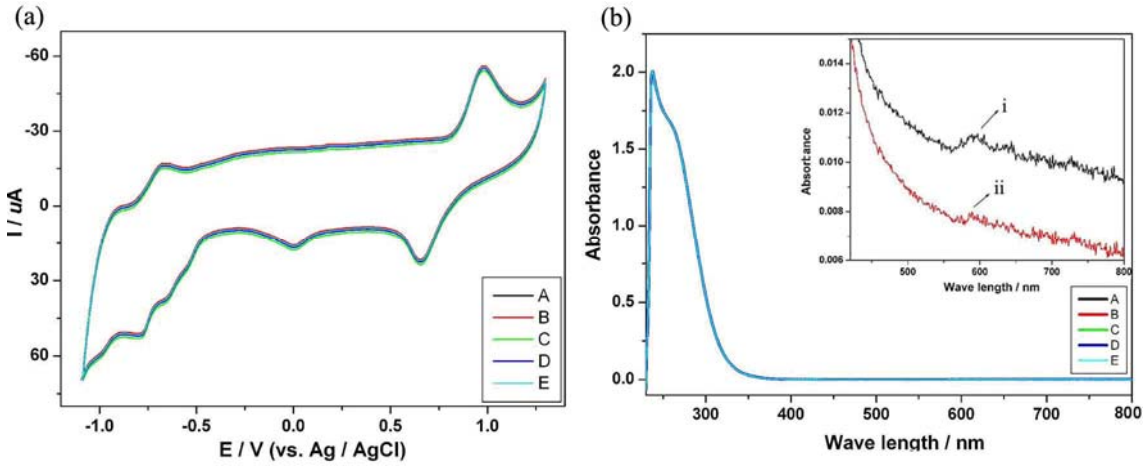

Fig. S13. (a) The cylicic voltammogram of **1** (10^{-3} M) in a pH 4 buffer solution (0.4M CH_3COONa + CH_3COOH). The CV curves were detected per 24 hours for five times; (b) The UV spectrum of **1** in the pH 4 buffer solution. The UV curves were detected per 24 hours for five times. The UV spectra (inset): (i) the UV-Vis spectrum of **1** (2.0 x 10^{-3} M) in the pH 4 buffer solution; (ii) the UV-Vis spectrum of the eluted solution of **1** coming out of the Sephadex G-50 (fine) column.

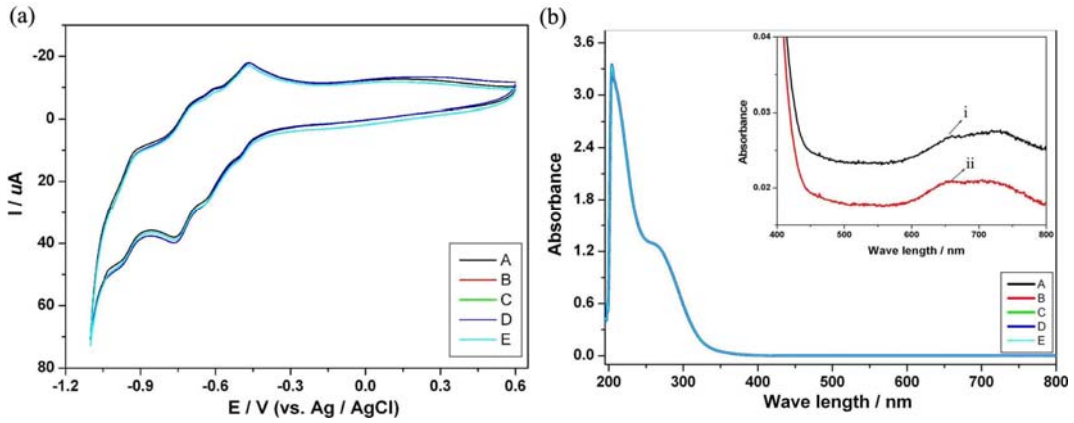

Fig. S14. (a) The cylicic voltammogram of **2** (10^{-3} M) in a pH 2.5 aqueous solution (1 M LiCl + 0.5 M H_2SO_4). The CV curves were detected per 24 hours for five times; (b) The UV spectrum of **2** in the pH 2.5 buffer solution. The UV curves were detected per 24 hours for five times. The UV spectra (inset): (i) the UV-Vis spectrum of **2** (2.0 x 10^{-3} M) in the pH 2.5 aqueous solution; (ii) the UV-Vis spectrum of the eluted solution of **2** coming out of the Sephadex G-50 (fine) column.

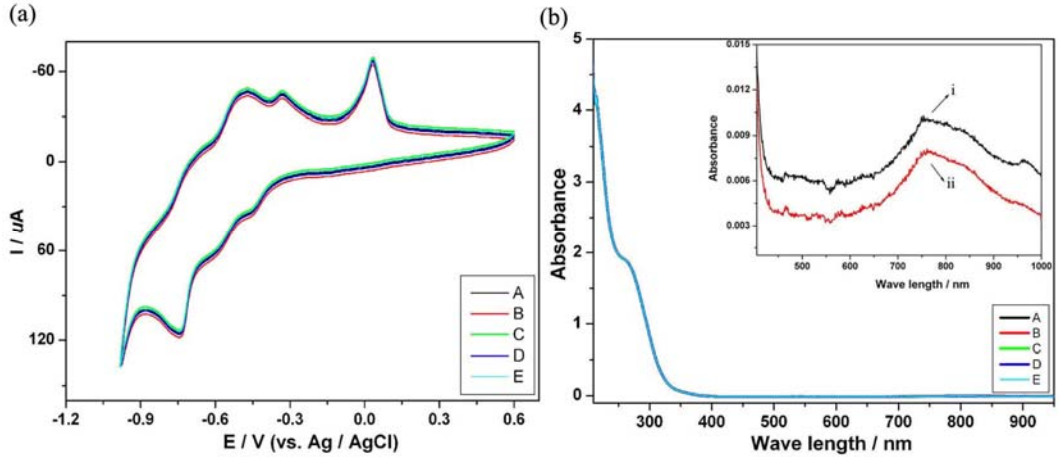

Fig. S15. (a) The cylicic voltammogram of **3** (10^{-3} M) in a pH 2.5 aqueous solution (1 M LiCl + 0.5 M H_2SO_4). The CV curves were detected per 24 hours for five times; (b) The UV spectrum of **3** in the pH 2.5 buffer solution. The UV curves were detected per 24 hours for five times; The UV spectra (inset): (i) the UV-Vis spectrum of **3** (2.0 x 10^{-3} M) in the pH 2.5 aqueous solution; (ii) the UV-Vis spectrum of the eluted solution of **3** coming out of the Sephadex G-50 (fine) column.

5. Electrochemistry and Electrocatalysis of 1-3

The electrochemical behaviors of compounds **1-3** and their electrocatalytic properties for nitrate were studied (Fig. S16-19). The cyclic voltammetric behavior for **1** in a pH 4 (0.4 M CH_3COONa+CH_3COOH) buffer solution exhibits four reduction peaks in the potential range of +1.3 ~ -1.2V and the mean peak potentials are 0.634 V, -0.029 V, -0.767 V and -0.997 V (vs. Ag/AgCl), respectively (see Fig. S16a). The first two reduction waves located at 0.634 V and -0.029 V and one single oxidation process (0.919 V) are attributed to the redox processes of the Mn^{II} centers.[1] The peaks at -0.767 V and -0.997 V are ascribed to the reduction process of W^{VI} centers.[2] When the scan rates were lower than 150 mV s^{-1}, the peak currents of W reduction wave (II) were proportional to the scan rates (see Fig. S17), indicating that the redox process on the glassy carbon (GC) electrode is surface-controlled.[3] Compound **1** displays electrocatalytic activity to reduce nitrate (Fig. S16b). On addition of modest amounts of nitrate, the two reduction peak currents of W increased while the corresponding oxidation peak currents dramatically decreased, suggesting that nitrate was reduced by the two reduced POM species.[4] It is also worth mentioning that the second reduced species of POM **1** exhibit better electrocatalytic activity, that is, the catalytic activity is enhanced with the increasing extent of POM reduction. In comparison, no reduction of nitrate took place on the GC electrode in the absence of compound **1**.

The electrochemical properties of compound **2** were detected in the 1 M LiCl + 0.5 M H_2SO_4 at pH 2.5 (Fig. S18a). Three redox peaks appear in the potential range -0.4 V to -1.1 V, and the mean peak potentials vs $E_{1/2}$ = (Epa + Epc)/2 are -0.5221 V, -0.7462 V and -0.9429 V (vs. Ag/AgCl). Compound **2** displays electrocatalytic

activity to reduce nitrate (see Fig. S18b). With the addition of nitrate, the last two reduction peak currents increased while the corresponding oxidation peak currents decreased, suggesting that nitrate was reduced by the last two reduced polyoxoanion species. Furthermore, the catalytic activities were enhanced with the increasing extent of the polyoxoanion ion reduction.

The electrochemical properties of compound **3** were also detected in the 1 M LiCl + 0.5 M H_2SO_4 at pH 2.5 (Fig. S19). Two redox peaks appear in the potential range 0.6 V to -1.0 V. The first one oxidation wave and their reduction counterparts, two reduction processes located at +0.019 and -0.141 V, respectively, are attributed to the redox processes of the Cu^{II} centers. The two reduction waves located at +0.019 and -0.141 V feature the two-step reduction of Cu^{II} to Cu^{0} through Cu^{I}. The other redox processes in the negative domain correspond to the redox of the W^{VI}.[3] Compound **3** displays good electrocatalytic activity to reduce nitrate (Fig. S19). On addition of modest amounts of nitrate, the last two reduction peak currents of W increased while the corresponding oxidation peak currents dramatically decreased, suggesting that nitrate was reduced by two reduced polyoxoanion species.[5] It was also noted that the second reduced species exhibit better electrocatalytic activity, that is, the catalytic activity is enhanced with increasing extent of polyoxoanion reduction.

1 B. Keita, P. Mialane, F. Sécheresse, P. Oliveira, L. Nadjo, *Electrochem. Commun.*, 2007, 9, 164.

2 (a) L. H. Bi, K. Foster, T. McCormac, E. Dempsey, *J. Electroanal. Chem.* 2007, 605, 24; (b) B. Keita, Y. W. Lu, L. Nadjo, R. Contant, *Electrochem. Commun.*, 2000, 2, 720; (c) B. Godin, Y. G. Chen, J. Vaissermann, L. Ruhlmann, M. Verdaguer, P. Gouzerh, *Angew. Chem. Int. Ed.*, 2005, 44, 3072.

3 L. Cheng, X. M. Zhang, X. D. Xi, B. F. Liu, S. J. Dong, *J. Electroanal. Chem.*, 1996, 407, 97.

4 M. Sadakane, E. Stechhan, Chem. Rev., 1998, 98, 219

5 (a) B. Keita, Y. W.i Lu, L. Nadjo, R. Contant, *Electrochem. Commun.,* **2000**, *2*, 720; (b) M. Sadakane, E. Stechhan, *Chem. Rev.*, **1998**, *98*, 219.

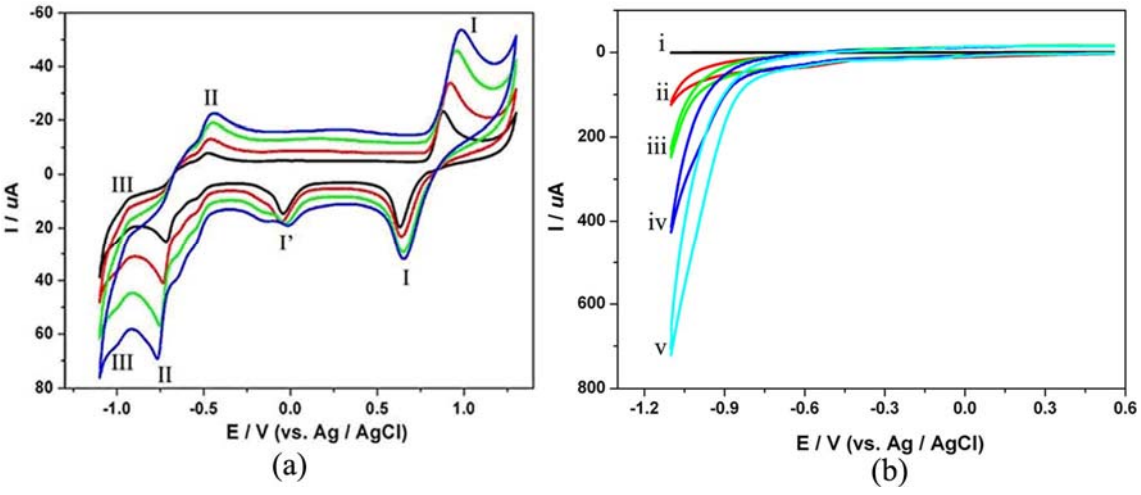

Fig. S16. (a) Cyclic voltammograms of 10^{-3} M **1** in the pH 4 (0.4 M CH_3COONa+CH_3COOH) buffer solution at the scan rates (from inner to outer: 10, 50, 100 and 150 mV s^{-1}); (b) Electrocatalysis of the reduction of NO_3^- in the presence of 10^{-3} M **1** at the scan rate of 200 mV s^{-1} with NO_3^- concentrations of 0.0 (ii), 2.0 (iii), 4.0 (iv) and 6 mM (v); (i) represents the cyclic voltammogram of the NO_3^- in the absence of **1**. The working electrode was glassy carbon; the reference electrode was Ag/AgCl.

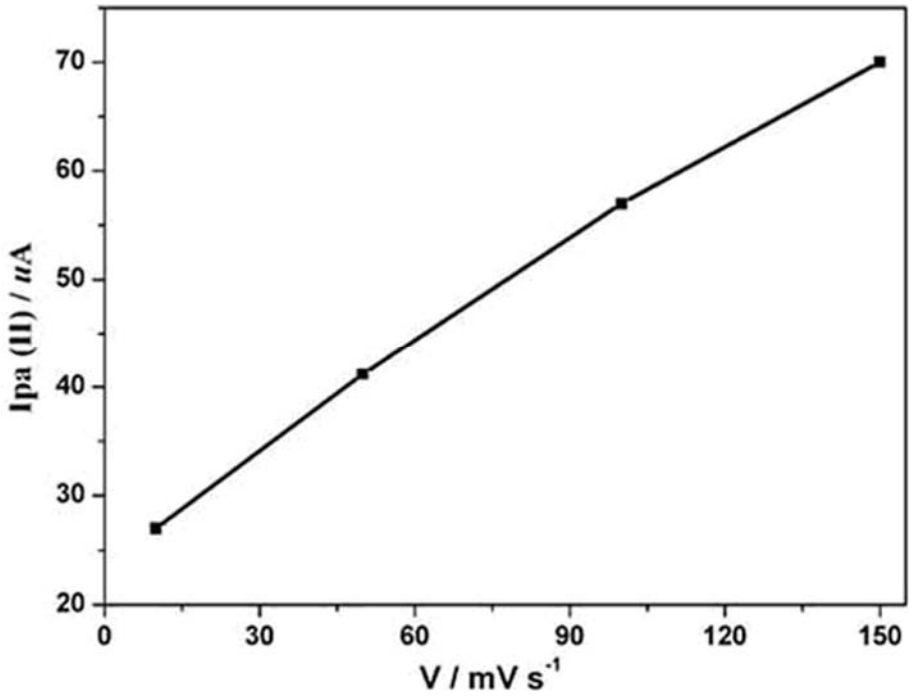

Fig. S17. The dependence of anodic peak II currents of **1** on scan rates.

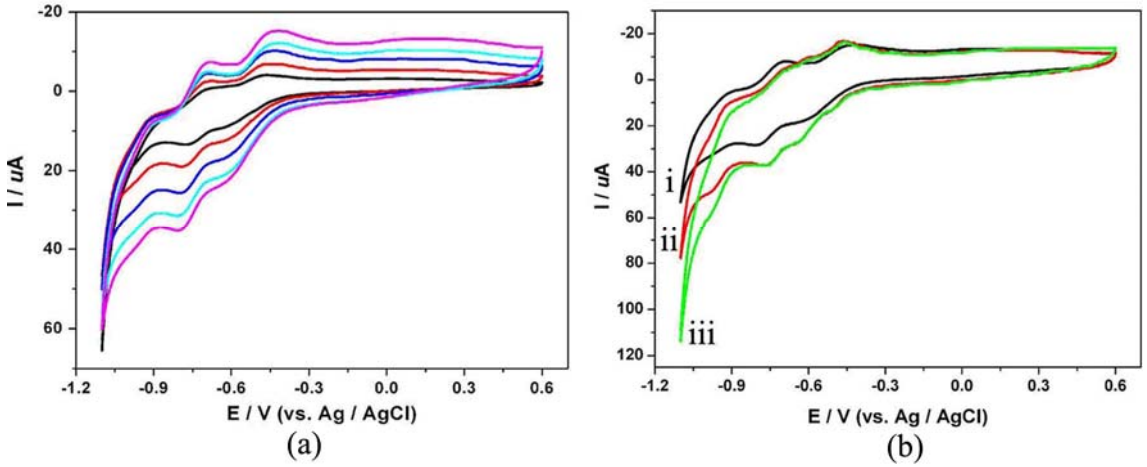

Fig. S18. (a) Cyclic voltammograms of **2** (10^{-3} M) in pH 2.5 solution at the scan rates of 10, 20, 50, 100 and 150 mV s^{-1} (from inner to outer); (b) Electrocatalysis of the reduction of NO_3^- in the presence of 10^{-3} M **2** in the pH 2.5 solution at the scan rate of 100 mV s^{-1}. The NO_3^- concentrations were 0.0 (i), 1.0 (ii) and 2.0 (iii) mM. The working electrode was glassy carbon; the reference electrode was Ag/AgCl.

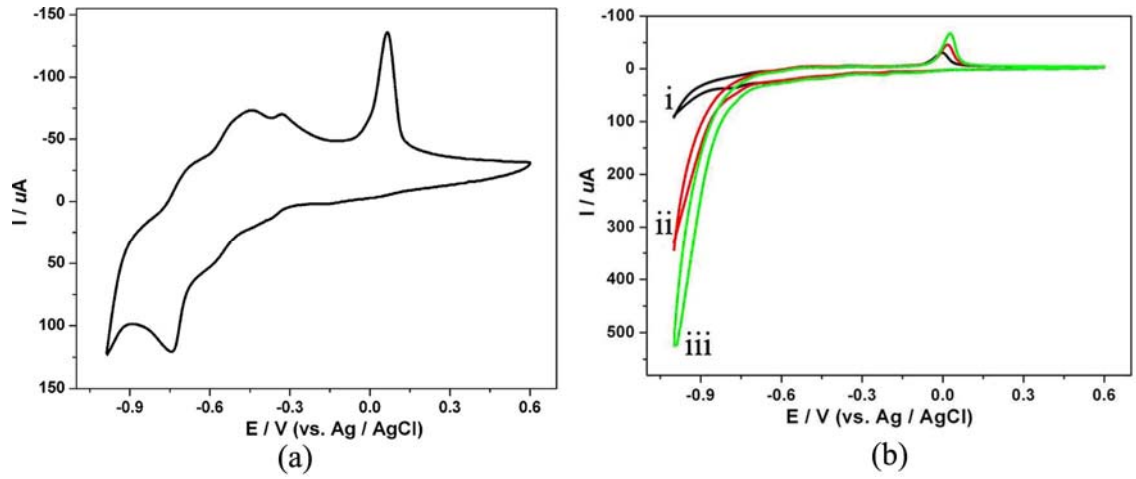

Fig. S19. (a) Cyclic voltammograms of 10^{-3} M **3** in the 1 M LiCl + 0.5 M H_2SO_4 in the pH 2.5 solution at the scan rate of 150 mV s^{-1}; (b) Electrocatalysis of the reduction of NO_3^- in the pH 2.5 solution at the scan rate of 100 mV s^{-1}. The NO_3^- concentrations were 0.0 (i), 2.0 (ii) and 5 (iii) mM. The working electrode was glassy carbon; the reference electrode was Ag/AgCl.

6. Magnetic properties of compounds 1-3

The magnetic susceptibilities (χ_M) of compounds **1-3** were measured in the temperature range of 2.0 – 300 K in a 0.1 T magnetic field (see Fig. S20). In all three χT *vs* T plots, the χT values slowly decrease from 300 K to 2 K. For **1**, the χT product of 8.95 cm^3 K mol^{-1} at 300 K is a little higher than the spin-only value (g = 2.0) of 8.75 cm^3 K mol^{-1} for two non-interacting Mn^{II} ions (S = 5/2). The $1/\chi$ vs T curve is in accordance with the Curie-Weiss law with C = 9.04 cm^3 K mol^{-1} and θ = -1.32 K, indicating a weak antiferromagnetic interaction in the whole crystal structure. For **2**, the $1/\chi$ vs T curve is well fitted with the Curie-Weiss law, resulting in a Curie constant of C = 4.2 cm^3 K mol^{-1}. Further, the Weiss temperature of θ = -1.51 K suggests a weak antiferromagnetic interaction in **2**. For **3**, the $1/\chi$ vs T curve is also well fitted with the Curie-Weiss law, leading to a Curie constant of 1.26 cm^3 K mol^{-1}. The Weiss temperature (θ) of -1.70 K indicates a weak antiferromagnetic interaction in **3**.

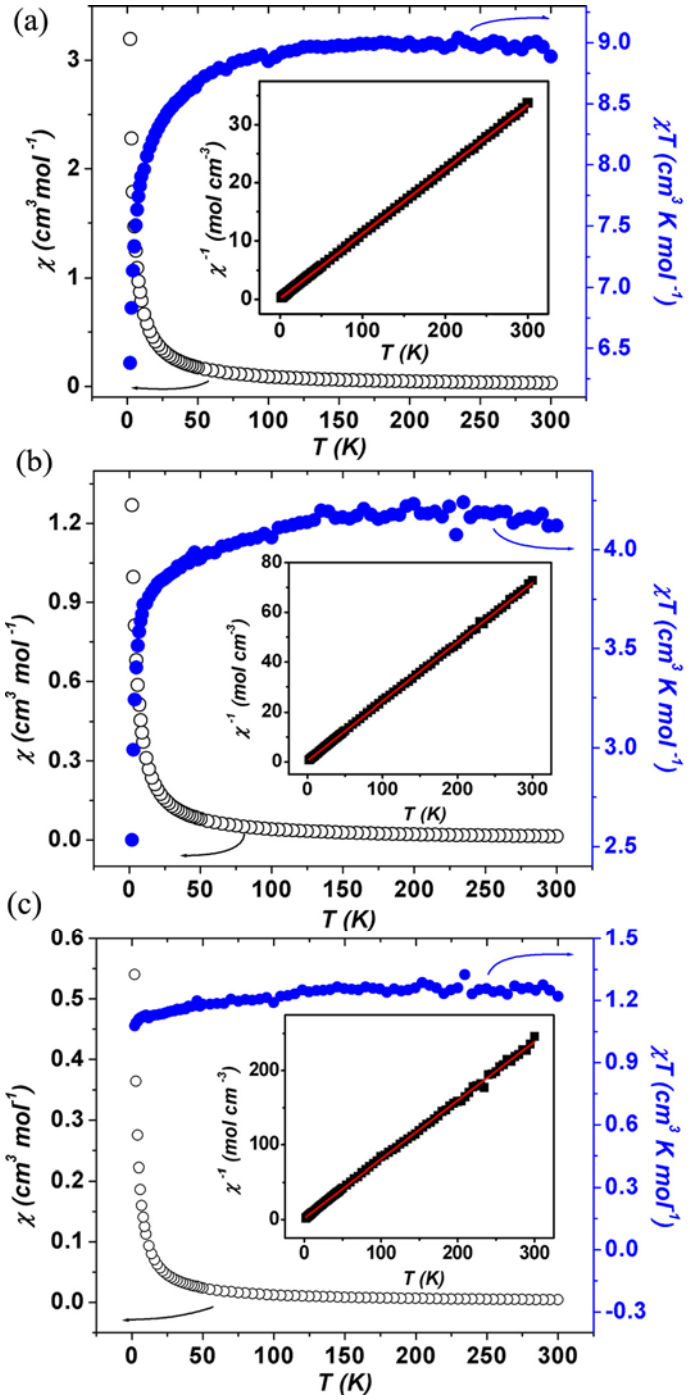

Fig. S20. Temperature dependence of χ (○) and χT (●) values and (inset) temperature dependence of reciprocal magnetic susceptibility χ^{-1} for **1** (a), **2** (b) and **3** (c).

7. Other Characterizations of Compounds 1-3

7.1. TG analyses.

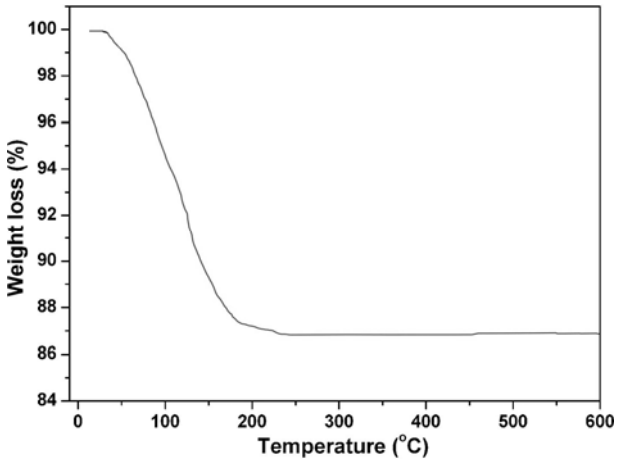

Fig. S21. The TG curve of compound **1**. The weight loss of 13.28% in the range of 45 ~ 235 °C is attributed to the loss of all lattice and coordinated water molecules in **1** (calcd. 13.23%).

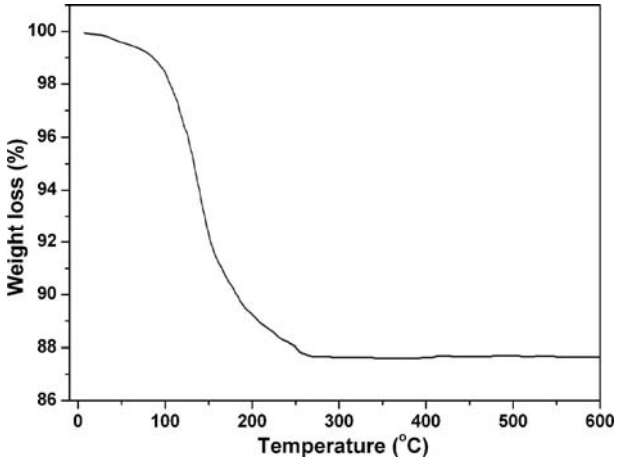

Fig. S22. The TG curve of compound **2**. The weight loss of 12.40% in the range of 30 ~ 270 °C is attributed to the loss of all lattice and coordinated water molecules (calcd. 12.34%).

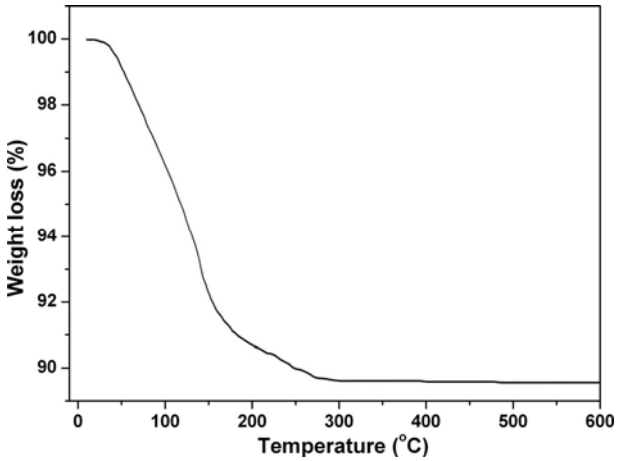

Fig. S23. The TG curve of compound **3**. The weight loss of 9.50 % in the range of 43 ~ 295 °C is attributed to the loss of all lattice and coordinated water molecules (calcd. 9.44 %).

7.2. IR spectra of compounds 1-3

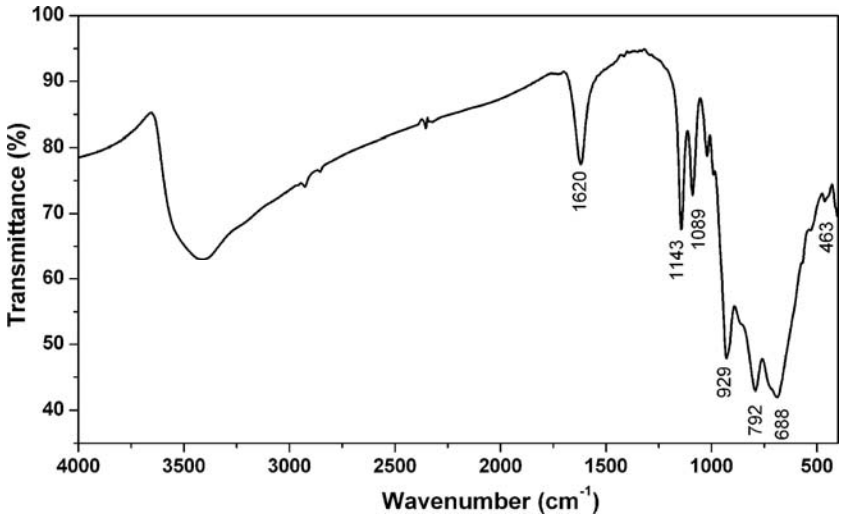

Fig. S24. IR spectrum for compound **1**.

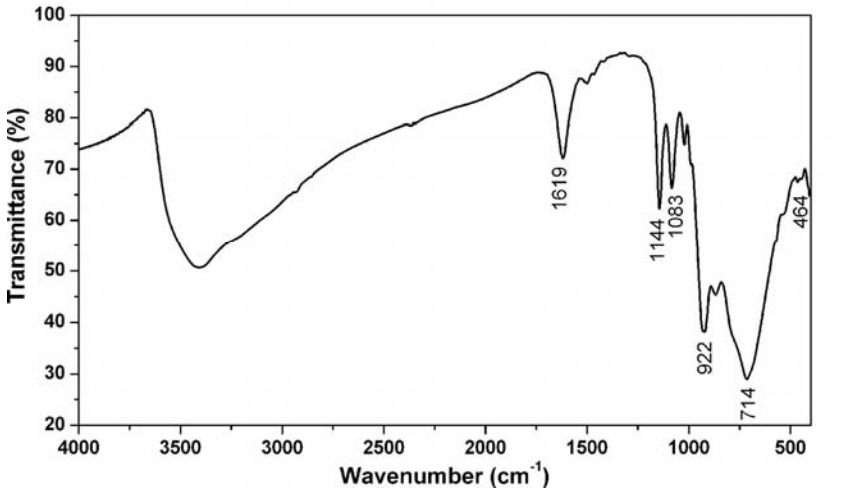

Fig. S25. IR spectrum for compound **2**.

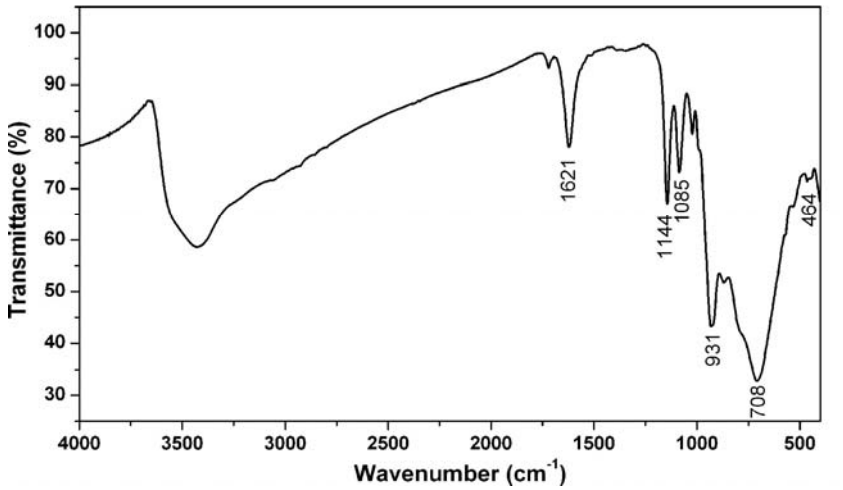

Fig. S26. IR spectrum for compound **3**.